Environmental Sciences Proceedings

MDPI

Proceedings

Reduction of Nitrogen Load in a Zootechnical Wastewater Using a Natural Chabazite Zeolite: An Investigation on Sorption Mechanisms †

Giulio Galamini *, Giacomo Ferretti, Valeria Medoro, Nicola Tescaro, Barbara Faccini and Massimo Coltorti

Department of Physics and Earth Science, University of Ferrara, via Saragat 1, 44122 Ferrara, Italy; frrgcm@unife.it (G.F.); mdrvlr@unife.it (V.M.); nicola.tescaro@student.unife.it (N.T.); fccbbr@unife.it (B.F.); clt@unife.it (M.C.)

* Correspondence: glmgli@unife.it

† Presented at the 4th EWaS International Conference: Valuing the Water, Carbon, Ecological Footprints of Human Activities, Online, 24–27 June 2020.

Published: 3 September 2020

Abstract: The use of zeolite-rich tuffs is a valid method for recovering nitrogen from wastewaters. This paper aims at describing the NH_4^+ adsorption processes of an Italian chabazite zeolite tuff used for the treatment of raw liquid swine manure. The effects of temperature, grain size and contact time were investigated. The isothermal analysis showed a multilayer adsorption behavior, well explained by the Harkins–Jura model, while kinetics was explained by pseudo-second-order, Elovich and intraparticle diffusion models. This study highlighted the complexity of the adsorption process from raw liquid manure, as well as the significant differences between tested particle sizes of the same zeolite tuff.

Keywords: ammonium adsorption; pig manure; natural zeolite tuff; chabazite; isotherm; kinetic; thermodynamic; wastewaters; agriculture

1. Introduction

The use of natural zeolite-rich tuffs for wastewater treatment is recognized as a valid method to reduce the inorganic cationic species like NH_4^+. Then, once saturated by NH_4^+, the zeolite tuff can be reused and employed as soil amendment or as growing media with many important advantages, as demonstrated by recent works [1–4].

The adsorption mechanisms of NH_4^+ from synthetic solutions prepared in laboratory were deeply investigated during the past twenty years [5–7]. However, a detailed description of NH_4^+ adsorption from a real zootechnical wastewater is, up to now, totally missing. Furthermore, most of the studies were conducted using clinoptilolite or heulandite tuffs, while chabazite ones were investigated far less.

In this paper, various experiments (following, as closely as possible, the procedures indicated by Wasielewski et al. [8]) are illustrated, with the aim to deeply characterize the adsorption mechanisms of NH_4^+ by an Italian chabazite-rich tuff (CHA) from a raw liquid swine manure. The experiments included the evaluation of temperature, contact time and particle size effects.

2. Materials and Methods

2.1. Materials, Experimental Design and Analytical Methods

The CHA was quarried in central Italy (Sorano, Grosseto province) and was purchased by Verdi S.p.a. company. The physico-chemical characteristics and the mineralogical composition of the used CHA is reported in Malferrari et al. [9]. Two grain sizes were selected for the experiments, a granular one (>0.7 and <2.0 mm; CHAg) and a μ-sized one (<62 μm; CHAμ); both were dried at 105 °C for 24 h before the beginning of the experiments.

The liquid swine manure was obtained from a local farmer in a 25 L tank. To improve the homogeneity of the liquid manure (rich in suspended solids), the sample was centrifuged at 4000 rpm for 8 min. The supernatant was collected to obtain the liquid phase for the experiments (centrifuged swine manure, CSM). The initial CSM's pH was 8.07 ± 0.03, while NH_4^+ concentration was 3140 ± 45 mg L^{-1}.

Isothermal adsorption experiments have been carried out at 13, 20 and 37 °C. Seven dosages of CHA, ranging from 0.5 to 12 g, were mixed with 50 mL of CSM into plastic bottles in three replicates and stirred in an orbital shaker at 200 rpm for 20 h. Samples without CHA were included (blanks) in order to evaluate the air stripping effect. Since pH measurements barely varied between 8.07 and 8.48 (optimum pH range for the adsorption of NH_4^+ by zeolites found by [10]), we decided not to further investigate the pH effects and to not buffer the CSM. After 20 h of shaking, the mixtures were centrifuged at 4000 rpm for 8 min and analyzed for their NH_4^+ concentration with an Ion Selective Electrode (ISE) Orion 95-12 connected to an Orion 4star pH-ISE benchtop (Thermo Fisher). NH_4^+ equilibrium adsorption capacity (q_e, mg g^{-1}) was determined by Equation (1):

$$q_e = \frac{(C_0 - (C_0 - C_b) - C_e) * V}{m} \quad (1)$$

where C_0 (mg L^{-1}) is the initial NH_4^+ concentration, C_b (mg L^{-1}) is the NH_4^+ concentration in blanks after 20 h, C_e (mg L^{-1}) is the concentration at equilibrium, V (L) is the volume of CSM and m (g) is the mass of the sorbent (CHA).

For the kinetic experiments, CHA was added to 0.5 L of CSM at a ratio of 0.1 g per mg NH_4-N in the batch (≅122 g) and mixed at a constant temperature of 20 °C, at a speed of 400 rpm, for 420 min. An aliquot of 10 mL was sampled at periodic intervals (5, 10, 20, 30, 45, 60, 120, 180, 270, 360 and 420 min) and immediately centrifuged at 4000 rpm for 4 min in order to separate the sorbent from the liquid fraction and stop the sorption processes. The batch volume was continuously reduced due to sampling, but it can be assumed that no change in the ratio of sorbent mass to the volume of CSM occurred because of the homogeneity of the mixture. Experiments were carried out in triplicates and a batch without zeolite (blank) was also included in the kinetic experiments in order to evaluate the air stripping effect. NH_4^+ concentration at time t (C_t, mg L^{-1}) was measured by ISE electrode as in the isothermal adsorption experiments. The time-dependent NH_4^+ loadings (q_t, mg g^{-1}) were calculated by Equation (1) replacing q_e and C_e with q_t and C_t, respectively. At 420 min, we considered that a "near-equilibrium" condition was achieved, thus it was assumed that $q_{t,420} \cong q_e$.

2.2. Data Analysis and Calculations

The equilibrium data were tested within the Harkins–Jura, Freundlich and Langmuir isotherms.

The Harkins–Jura linear isotherm can be expressed by Equation (2) [11]:

$$\frac{1}{{q_e}^2} = \beta \ \ln(C_e) + \ \alpha \quad (2)$$

where q_e is the equilibrium adsorption capacity (mg g^{-1}), C_e is the equilibrium sorbate concentration (mg L^{-1}), and α and β are constants; in particular, β is linked to the specific surface area of the sorbent.

The Freundlich model is reported by Equation (3) [12]:

$$q_e = K_F \times C_e^{1/n} \quad (3)$$

where K_F (L g^{-1}) is the Freundlich constant and n is the adsorption capacity.

The Langmuir model [13] in its linear form can be expressed by Equation (4):

$$\frac{1}{q_e} = \frac{1}{q_{max} K_L} \frac{1}{C_e} + \frac{1}{q_{max}} \quad (4)$$

where q_{max} (mg g^{-1}) is the maximum monolayer adsorption capacity and K_L is the Langmuir constant (L mg^{-1}).

Kinetic data were analyzed applying pseudo-first-order (PFO), pseudo-second-order (PSO), intraparticle diffusion (ID) and Elovich equations.

The PFO [14] can be described by Equation (5) [15]:

$$\ln(q_e - q_t) = \ln(q_e) - \frac{k_1}{2.303} t \quad (5)$$

where q_e and q_t are the equilibrium adsorption capacity and the adsorption capacity at time t (mg g^{-1}), respectively, t is the contact time (min) and k_1 is the PFO rate constant (min^{-1}).

The PSO proposed by Ho et al. [16] is expressed in linear form by Equation (6):

$$\frac{t}{q_t} = \frac{1}{q_e} t + \frac{1}{h} \quad (6)$$

where h is the initial adsorption rate (mg g^{-1} min^{-1}). From the experimental data, it is possible to calculate h when q_t/t approaches 0: $h = k_2/q_e^2$, where k_2 is the PSO rate constant[17].

The ID is a diffusion-controlled process described by Equation (7) [18]:

$$q_t = k_{ID} t^{0.5} + C \quad (7)$$

where K_{ID} is the intraparticle diffusion rate constant (mg g^{-1} $min^{-0.5}$) and an intercept C proportional to the thickness of the boundary layer, as reported by [19].

The Elovich model can be expressed in linear form by Equation (8) [15].

$$q_t = \left(\frac{2.3}{\alpha}\right) \ln(t + t_0) - \left(\frac{2.3}{\alpha}\right) \ln(t_0) \quad (8)$$

where α is the initial adsorption rate constant [20]. The dimensionless form of the Elovich equation (Equation (9)) permits the calculation of R_E, which is an approaching-equilibrium parameter, proportional to the tendency of the system to achieve equilibrium conditions [21].

$$\frac{q_t}{q_{ref}} = R_E \ln \left(\frac{t}{t_{ref}}\right) + 1 \quad (9)$$

Thermodynamic parameters were calculated using the van't Hoff relation (Equation (10)) [22]:

$$\ln(K_{eq}) = -\frac{\Delta H}{R} \frac{1}{T} + \frac{\Delta S}{R} \quad (10)$$

where K_{eq} is the thermodynamic equilibrium constant, ΔH is the enthalpy change (J mol^{-1}), ΔS is the entropy change (J K^{-1} mol^{-1}), R is the universal gas constant (J K^{-1} mol^{-1}) and T is the temperature (K). K_{eq} has been derived by $K_{eq} = \delta K_d$, where K_d is the distribution coefficient ($K_d = q_e/C_e$; mL g^{-1}) [6,23], and δ is the density of CSM (~1.009 g mL^{-1}). The Gibbs free energy change (ΔG, kJ mol^{-1}) was determined by the Gibbs–Helmholtz equation (Equation (11)):

$$\Delta G = \Delta H - T\Delta S \quad (11)$$

3. Results and Discussions

3.1. Isotherms

Isotherm parameters are reported in Table 1, while equilibrium condition plots are reported in Figure 1.

Table 1. Parameters calculated by Harkins–Jura, Freundlich and Langmuir isotherms (Equations (2), (3) and (5), respectively) for CHAμ and CHAg, at temperatures T = 286, 293 and 307 K (13, 20 and 37 °C).

Sorbent	Temp.	Harkins–Jura			Freundlich			Langmuir		
	T	R^2	α	β	R^2	K_F	n	R^2	K_L	q_{max}
	(K)	(-)	(g^2 mg^{-2})	(g^2 L mg^{-3})	(-)	(L g^{-1})	(-)	(-)	(L mg^{-1})	(mg g^{-1})
CHAμ	286	0.973	0.057	−0.015	0.904	0.14	1.67	0.878	3.98×10^{-4}	29.5 (2.9)
	293	0.931	0.045	−0.012	0.853	0.66	2.55	0.860	10.27×10^{-4}	19.6 (1.0)
	310	0.920	0.051	−0.013	0.896	0.77	2.71	0.911	12.03×10^{-4}	18.1 (0.7)
CHAg	286	0.876	0.109	−0.028	0.826	0.45	2.68	0.798	9.12×10^{-4}	12.0 (0.7)
	293	0.937	0.057	−0.015	0.937	0.56	2.55	0.954	7.40×10^{-4}	18.9 (0.6)
	310	0.826	0.063	−0.016	0.826	0.95	3.23	0.843	13.03×10^{-4}	14.0 (0.6)

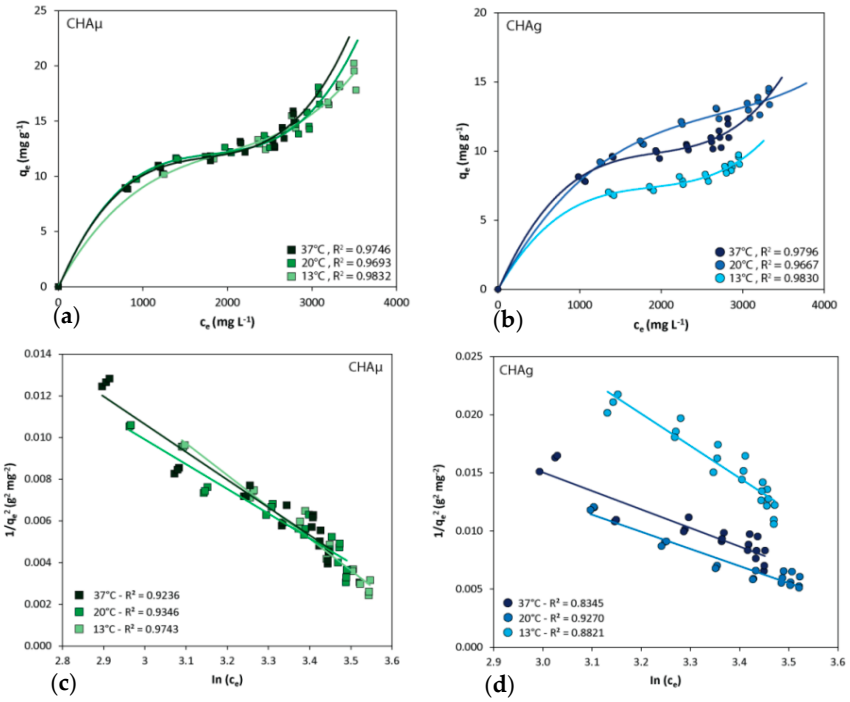

Figure 1. (**a**) q_e against C_e for CHAμ at 13, 20 and 37 °C; (**b**) q_e against C_e for CHAg at 13, 20 and 37 °C; (**c**) In(C_e) against $1/q_e^2$ (Harkins–Jura isotherms, Equation (2)) for CHAμ; (**d**) In(C_e) against $1/q_e^2$ (Harkins–Jura isotherms, Equation (2)) for CHAg.

Both CHAμ and CHAg have shown curves of the L3 type in accordance with the classification proposed by Giles [24]. The presence of a "semi-flat" region (Figure 1a,b) in the middle of the curves means that a saturation condition is beginning to occur associated with the formation of a monolayer, but, at high C_e (right end of the curves), the increase in q_e demonstrates the renewed availability of exchange sites for NH_4^+ cations [24]. This behavior (multi-layer formation) has been observed for both CHAμ and CHAg and it starts at dosages ≤6% of CHA. The multilayer adsorption is not in agreement with Langmuir monolayer assumption [11] but it is in accordance with the other two models proposed, in fact, Harkins–Jura was found to be the best model (R^2 between 0.826 and 0.973). Temperature seems to not significantly affect the sorption for CHAμ (Figure 1a,c), but it has a

more relevant effect in the case of CHAg (Figure 1b,d); in particular, the best adsorption performances were obtained at 20 °C, whereas the worst were obtained at at 13 °C.

3.2. Kinetics

As pointed out by Simonin [25], in kinetic analysis, it is appropriate to take into account only data sufficiently far from equilibrium. For this reason, only data with a fractional uptake F(t) < 85%, calculated as $F(t) = q(t)/q_e$ [25], were chosen.

The PFO model showed bad correlation with respect to the other kinetic models applied, while the PSO model has shown high R^2 values (Table 2), but the q_e calculated ($q_{e,2}$) are slightly different from the real measured values (8.74 and 6.37 mg g^{-1} for CHAμ and CHAg, respectively). The Elovich model has shown a good correlation with the experimental data, in particular regarding CHAg. R_E values indicate that CHAg approaches equilibrium conditions more slowly than CHAμ.

Table 2. Pseudo First Order, Pseudo Second Order and Elovich parameters (see Section 2.2 for detailed description) for CHAμ and CHAg and the relative R^2 values.

Sorbent	PFO			PSO				Elovich		
	R^2	k_1	$q_{e,1}$	R^2	k_2	$q_{e,2}$	h	R^2	α	R_E
	(-)	(min^{-1})	(mg g^{-1})	(-)	(g mg^{-1} min^{-1})	(mg g^{-1})	(mg g^{-1} min^{-1})	(-)	(mg g^{-1} min^{-1})	(-)
CHAμ	0.682	0.011	5.38	0.977	0.022	6.98	1.665	0.929	1.182	0.282
CHAg	0.890	0.015	4.86	0.993	0.014	5.60	0.566	0.985	0.820	0.524

The diffusion dynamics of NH_4^+ have shown different behaviours between CHAg and CHAμ (Figure 2); in particular, the ID plot for CHAμ has shown only a straight line with an intercept C (Equation (7)) ~ 4, while CHAg has clearly shown two ID lines, correlated with a rapid change of NH_4^+ diffusion that begins after about 60 min after the contact with CSM.

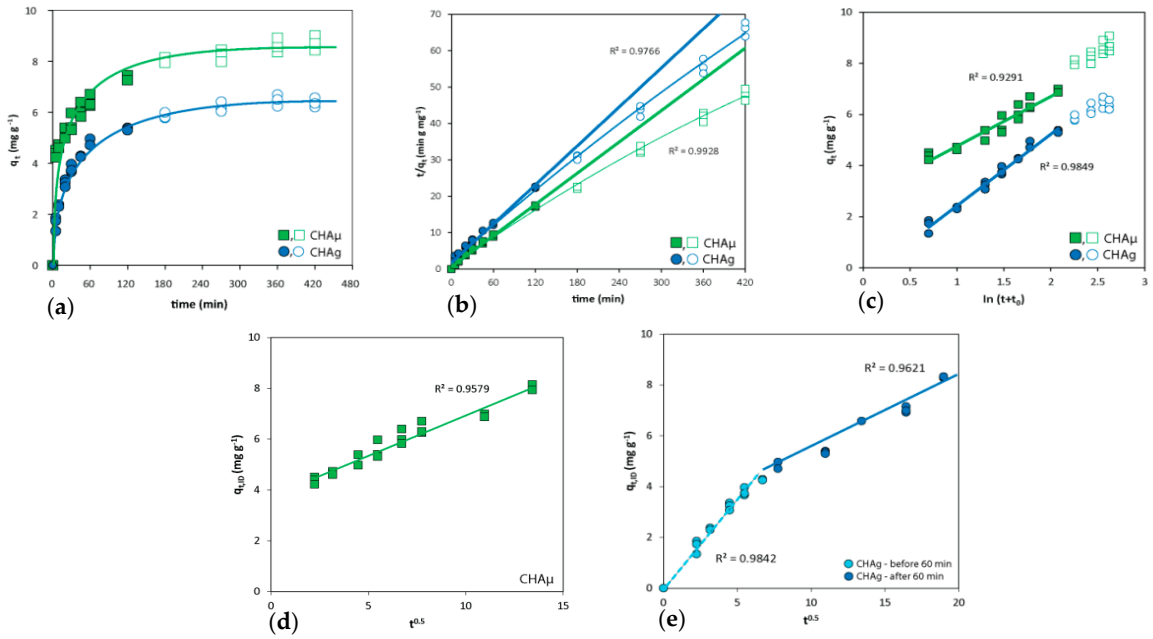

Figure 2. Kinetic graphics. Full dots are F(t) < 85% data (data considered in the kinetic analyzes); empty dots are F(t) > 85% data (excluded from the model fitting): (**a**) q_t against t; (**b**) t/q_t against t (PSO model, Equation (6)), only straight thick lines represent the PSO model while thinner lines also represent data excluded (with F(t) > 85%); (**c**) $(t + t_0)$ versus q_t (Elovich model, Equation (8)); (**d**) $t^{0.5}$ against $q_{t,ID}$ (ID model, Equation (7)) for CHAμ; (**e**) $t^{0.5}$ against $q_{t,ID}$ (ID model, Equation (7)) for CHAg; the graph shows two distinct regions with different ID parameters; the first is represented by light blue dots, while the second is represented by dark blue dots.

In the first region of the CHAg ID plot (Figure 2e), which represents about the first 60 min of contact with CSM, the intercept value was near zero (C = 0.17), demonstrating that the adsorption is mainly governed by ID. Thus, during this first stage, external-surface adsorption and macropore diffusion occurs and a thin boundary layer develops. The thickness of this boundary layer is proportional to the C value and hence it was thin during the first 60 min [19].

After one hour, the adsorption layers thicken significantly (C = 2.24), suggesting that the NH_4^+ penetrates more slowly inside the internal structure and the micropores. This is validated by K_{ID} values that after 60 min are lower (slower diffusion) with respect to values calculated from the first hour (Table 3).

Table 3. ID parameters for CHAμ and CHAg; CHAg has two distinct patterns, before and after 60 min.

Sorbent		ID Model		
		R^2	K_{ID}	C
		(-)	(mg g^{-1} $min^{-0.5}$)	(mg g^{-1})
CHAμ		0.958	0.32	3.75
CHAg	before 60 min	0.984	0.63	0.17
	after 60 min	0.962	0.31	2.24

After about an hour of contact with CSM, the slope K_{ID} of CHAg reaches values similar to the one of CHAμ (0.31 and 0.32, respectively) (Table 3).
For CHAμ, the high value of C (C = 3.75) indicates the formation of an adsorption layer thicker than the one developed by CHAg in the second region of the graph (C = 2.24) (Figure 2d,e).

A plausible hypothesis is that because of the considerably higher surface area of CHAμ, the formation of an adsorption layer is immediate because of a negligible macropore diffusion (too high C values for ID). However, from the data obtained, a very fast ID within the first 5 min cannot be totally excluded.

3.3. Thermodynamics

The thermodynamic parameters, reported in Table 4, show positive values for ΔH for both CHAμ and CHAg, indicating endothermal conditions, with significantly higher values for CHAg. Because ΔH > 0, the amount of energy in the liquid–solid adsorption surfaces increases during NH_4^+ adsorption; thus, the NH_4^+ cationic exchange processes need energy from the liquid phase in order to occur. While many authors have observed exothermic conditions (ΔH < 0) [6,22,26], others have calculated positive values of ΔH [8,19]. In all these studies, the nature of the employed materials (zeolite tuff and solutions) varies significantly; this may explain the differences in thermodynamic parameters.

Table 4. Thermodynamic parameters for CHAμ and CHAg calculated by the isothermal data at the temperatures of 286, 293 and 310 K (13, 20 and 37 °C, respectively); see paragraph 2.5 for details.

Sorbent	Temperature	ΔH	ΔS	ΔG
	(K)	(J mol^{-1})	(J K^{-1} mol^{-1})	(kJ mol^{-1})
CHAμ	286	2124	13.7	−1.80
	293	2091	13.8	−1.96
	310	2146	13.6	−2.06
CHAg	286	2654	11.9	−0.74
	293	2343	13.0	−1.46
	310	2479	12.6	−1.42

ΔS is also positive, indicating that NH_4^+ adsorption is a directional process and that the NH_4^+ cations captured in the adsorption layers are in a more chaotic disposition with respect to the ones in

the liquid phase. NH_4^+ adsorption is a spontaneous reaction ($\Delta G < 0$) for all the temperatures investigated. ΔG values are significantly lower for CHAμ than CHAg.

4. Conclusions

In this work, the adsorption of NH_4^+ from a raw liquid swine manure by chabazite-zeolite tuff was deeply characterized. The equilibrium curve was of the L3 type and demonstrated that, to obtain maximum adsorption by the zeolite tuff, it is necessary to use low dosages of adsorbant (<6%). A clear temperature effect was not observed for the μ-sized one, while the granular one has shown deficient capacity at lower temperatures. Kinetic analyses have shown that the μ-sized zeolite tuff approaches equilibrium faster than the granular one. ID plots have shown significant differences between the two grain sizes studied. For the granular one, the presence of two distinct regions in the graph demonstrates a change in diffusion dynamics during adsorption, with an initial rapid diffusion inside the macropores and on the external surfaces, followed by a slower diffusion inside the micropores.

The outcomes of this work highlighted the complexity of the sorption mechanisms in a complex matrix such as raw liquid manure in comparison to other studies performed on synthetic solutions. On the other hand, the studied Italian chabazite-zeolite tuff was confirmed as a valid material for the treatment of animal liquid manure and these data can be of high value for future application at the field scale.

Author Contributions: Conceptualization, G.G. and G.F.; methodology, G.G. and G.F.; formal analysis, G.G., G.F., V.M., N.T.; investigation, G.G.; resources, B.F. and M.C.; data curation, G.G.; writing—original draft preparation, G.G.; writing—review and editing, G.F., B.F., M.C.; supervision, G.F., M.C. All authors have read and agree to the published version of the manuscript.

Funding: This research received no external funding.

Acknowledgments: We gratefully thank the Miotto Giuliano company for the swine manure supply and Maurizio Bellettato (FerraraBio s.r.l) for the furniture of the zeolite tuff.

Conflicts of Interest: The authors declare no conflict of interest.

References

1. Ferretti, G.; Galamini, G.; Medoro, V.; Coltorti, M.; Giuseppe, D. Di; Faccini, B. Impact of Sequential Treatments with Natural and Na-Exchanged Chabazite Zeolite-Rich Tuff on Pig-Slurry Chemical Composition. *Water* **2020**, *12*, 310.
2. Ferretti, G.; Faccini, B.; Vittori Antisari, L.; Di Giuseppe, D.; Coltorti, M. 15N Natural Abundance, Nitrogen and Carbon Pools in Soil-Sorghum System Amended with Natural and NH4+-Enriched Zeolitites. *Appl. Sci.* **2019**, *9*, 4524.
3. Ferretti, G.; Keiblinger, K.M.; Zimmermann, M.; Di Giuseppe, D.; Faccini, B.; Colombani, N.; Mentler, A.; Zechmeister-Boltenstern, S.; Coltorti, M.; Mastrocicco, M. High resolution short-term investigation of soil CO2, N2O, NOx and NH3 emissions after different chabazite zeolite amendments. *Appl. Soil Ecol.* **2017**, *119*, 138–144.
4. Faccini, B.; Di Giuseppe, D.; Ferretti, G.; Coltorti, M.; Colombani, N.; Mastrocicco, M. Natural and NH4+-enriched zeolitite amendment effects on nitrate leaching from a reclaimed agricultural soil (Ferrara Province, Italy). *Nutr. Cycl. Agroecosystems* **2018**, *110*, 327–341.
5. Lin, L.; Lei, Z.; Wang, L.; Liu, X.; Zhang, Y.; Wan, C.; Lee, D.J.; Tay, J.H. Adsorption mechanisms of high-levels of ammonium onto natural and NaCl-modified zeolites. *Sep. Purif. Technol.* **2013**, *103*, 15–20.
6. Saltali, K.; Sari, A.; Aydin, M. Removal of ammonium ion from aqueous solution by natural Turkish (Yi{dotless}ldi{dotless}zeli) zeolite for environmental quality. *J. Hazard. Mater.* **2007**, *141*, 258–263.
7. Eslami, M.; Khorassani, R.; Coltorti, M.; Malferrari, D.; Faccini, B.; Ferretti, G.; Di Giuseppe, D.; Fotovat, A.; Halajnia, A. Leaching behaviour of a sandy soil amended with natural and NH4+ and K+ saturated clinoptilolite and chabazite. *Arch. Agron. Soil Sci.* **2018**, *64*, 1142–1151.
8. Wasielewski, S.; Rott, E.; Minke, R.; Steinmetz, H. Evaluation of Different Clinoptilolite Zeolites as Adsorbent for Ammonium Removal from Highly Concentrated Synthetic Wastewater. *Water* **2018**, *10*, 584.

9. Malferrari, D.; Laurora, A.; Brigatti, M.F.; Coltorti, M.; Di Giuseppe, D.; Faccini, B.; Passaglia, E.; Vezzalini, M.G. Open-field experimentation of an innovative and integrated zeolitite cycle: Project definition and material characterization. *Rend. Lincei* **2013**, *24*, 141–150.
10. Huang, H.; Xiao, X.; Yan, B.; Yang, L. Ammonium removal from aqueous solutions by using natural Chinese (Chende) zeolite as adsorbent. *J. Hazard. Mater.* **2010**, *175*, 247–252.
11. Shanavas, S.; Salahuddin Kunju, A.; Varghese, H.T.; Yohannan Panicker, C. Comparison of Langmuir and Harkins-Jura Adsorption Isotherms for the Determination of Surface Area of Solids: Oriental Journal of Chemistry. *Orient. J. Chem.* **2011**, *27*, 245–252.
12. Dada, A.O. Langmuir, Freundlich, Temkin and Dubinin–Radushkevich Isotherms Studies of Equilibrium Sorption of Zn 2+ Unto Phosphoric Acid Modified Rice Husk. *IOSR J. Appl. Chem.* **2012**, *3*, 38–45.
13. Langmuir, I. The adsorption of gases on plane surfaces of glass, mica and platinum. *J. Am. Chem. Soc.* **1918**, *40*, 1361–1403.
14. Lagergren, S.Y.; Sven, K. Zurtheorie der sogenannten adsorption gelösterstoffe. *K. Sven. Vetenskapsakademiens. Handl.* **1898**, *24*, 1–39.
15. Qiu, H.; Lv, L.; Pan, B.-C.; Zhang, Q.-J.; Zhang, W.-M.; Zhang, Q.-X. Critical review in adsorption kinetic models *. *J Zhejiang Univ Sci A* **2009**, *10*, 716–724.
16. Ho, Y.S.; McKay, G. Pseudo-second order model for sorption processes. *Process Biochem.* **1999**, *34*, 451–465.
17. Ho, Y.S. Review of second-order models for adsorption systems. *J. Hazard. Mater.* **2006**, *136*, 681–689.
18. Wu, F.C.; Tseng, R.L.; Juang, R.S. Initial behavior of intraparticle diffusion model used in the description of adsorption kinetics. *Chem. Eng. J.* **2009**, *153*, 1–8.
19. Widiastuti, N.; Wu, H.; Ang, H.M.; Zhang, D. Removal of ammonium from greywater using natural zeolite. *Desalination* **2011**, *277*, 15–23.
20. Ho, Y.S.; McKay, G. A Comparison of chemisorption kinetic models applied to pollutant removal on various sorbents. *Process Saf. Environ. Prot.* **1998**, *76*, 332–340.
21. Wu, F.C.; Tseng, R.L.; Juang, R.S. Characteristics of Elovich equation used for the analysis of adsorption kinetics in dye-chitosan systems. *Chem. Eng. J.* **2009**, *150*, 366–373.
22. Gunay, A. Application of nonlinear regression analysis for ammonium exchange by natural (Bigadiç) clinoptilolite. *J. Hazard. Mater.* **2007**, *148*, 708–713.
23. Gupta, S.; Bhattacharyya, K.G. Interaction of metal ions with clays: I. A case study with Pb(II). *Appl. Clay Sci.* **2005**, *30*, 199–208.
24. Giles, C.H.; MacEwan, T.H.; Nakhwa, S.N.; Smith, D. 786. Studies in adsorption. Part XI. A system of classification of solution adsorption isotherms, and its use in diagnosis of adsorption mechanisms and in measurement of specific surface areas of solids. *J. Chem. Soc.* **1960**, *111*, 3973–3993.
25. Simonin, J.P. On the comparison of pseudo-first order and pseudo-second order rate laws in the modeling of adsorption kinetics. *Chem. Eng. J.* **2016**, *300*, 254–263.
26. Aydın Temel, F.; Kuleyin, A. Ammonium removal from landfill leachate using natural zeolite: kinetic, equilibrium, and thermodynamic studies. *Desalin. Water Treat.* **2016**, *57*, 23873–23892.